Scientific Research Report

Establishment of an Osteoradionecrosis Model and its Mechanism Via Single Ionizing Radiation Exposure

Yuetong Wang [a,b,#], Xian Wang [a,b,#], Zhiqing Liu [a,b], Yuetao Li [a,b], Haoyu Lu [a,b], Dongqin Mo [a,b], Daiyou Wang [a,b*]

[a] College & Hospital of Stomatology, Guangxi Medical University, Nanning, Guangxi, P.R. China
[b] Guangxi Key Laboratory of Oral and Maxillofacial Rehabilitation and Reconstruction, Nanning, Guangxi, P.R. China

ARTICLE INFO

Article history:
Received 5 December 2024
Received in revised form
28 February 2025
Accepted 6 March 2025
Available online xxx

Key words:
Animal model
Radiotherapy
Osteoradionecrosis
Ionizing radiation
Fibrosis
Vascular injury

ABSTRACT

Introduction and Aims: The aim of this study was to establish a reliable model of osteoradionecrosis of the mandible in New Zealand white rabbits and systematically examine the impacts of different radiation doses on mandibular tissue, as well as to appraise the inducing role of tooth extraction in the pathogenesis of the disease.

Method: In this research, 16 New Zealand white rabbits were randomly allocated to the control group, the 16Gy group, the 18Gy group, and the 20Gy group with a single high-dose radiation. Two weeks after radiotherapy, the teeth were extracted, and the animals were sacrificed four weeks later. Micro CT, scanning electron microscopy, HE staining, Masson staining, TRAP staining, TUNEL staining, and immunohistochemical staining were employed to verify the modelling status and damage mechanism.

Results: Research findings show that, compared to the control group, rabbits exposed to 18Gy and 20Gy radiation doses exhibited significant bone necrosis after tooth extraction. Key observations included extensive bone tissue necrosis, increased osteoclasts ($P < .05$), reduced vascularization ($P < .001$), exacerbated fibrosis ($P < .001$), decreased bone density, disrupted trabecular structure, and damaged bone surface microstructure. In contrast, the 16Gy group showed some bone damage but did not meet bone necrosis criteria.

Conclusion: This study established an animal model appropriate for inducing ORNJ with a single large dose of radiation.

Clinical Relevance: This work provides a solid experimental basis and a theoretical framework for further studies of ORNJ pathogenesis in particular to explore effective preventive and clinical treatment strategies.

Introduction

Head and neck cancer has emerged as the sixth most prevalent malignancy globally, with an ascending incidence rate primarily influenced by the intake of noxious substances such as tobacco, alcohol, and betel nut, along with the aging of the population.[1] Among these neoplasms, over 90% are squamous cell carcinomas. Sadly, the majority of patients present with locally advanced disease at the time of diagnosis, accompanied by regional lymph node or distant metastasis. Radiation therapy assumes a crucial role in treatment. According to statistics, approximately two-thirds of patients with head and neck malignancies require a combination of surgery and radiation therapy.[2] Radiation therapy exerts its effects by directly targeting tumour cells with high-energy rays, inhibiting their growth and division to achieve therapeutic goals. However, although this approach is effective, its side effects cannot be disregarded. Among them, osteoradionecrosis of the jaws (ORNJ), as the most serious complication of head and neck radiation therapy, can induce severe pain, ulcers, exposure of bone necrosis, and pathological fractures, and even lead to death, which has a profound impact on the prognosis and quality of life of patients.[3]

The pathogenesis of ORNJ is intricate and may encompass multiple factors, such as radiation-induced damage to bone

* *Corresponding author*. College & Hospital of Stomatology, Guangxi Medical University, No.10 Shuangyong Road, Nanning, Guangxi, 530021, P.R. China.
E-mail address: wangdaiyou@sina.com (D. Wang).
Daiyou Wang: http://orcid.org/0000-0002-7789-0756

# These authors should be considered joint first author.

https://doi.org/10.1016/j.identj.2025.03.006

tissue cells, vascular impairment, and reduced capacity for healing. Initially, scholars postulated that ORNJ was caused by bacteria invading the jawbone through wounds and initiating a chronic infectious disease.[4] Subsequently, researchers detected the presence of deep anaerobic bacteria in radiation-necrotic jawbones via DNA hybridization, a finding that seemingly lent further credence to this perspective.[5] In 1983, Marx initially proposed the "3Hs" theory, which postulated that radiation-induced reduction in blood supply leads to tissue hypoxia and cell death, disturbances in metabolism and tissue homeostasis, and ultimately non-healing of wounds.[6] In 2004, Delanian and Lefaix put forward the theory of radiation-induced fibrous atrophy (RIF), and they contended that the development process of ORNJ encompasses three successive progressive stages: the pre-fibrotic stage, the fibrotic stage, and the fibroatrophic stage, involving endothelial cell alterations, abnormal proliferation of fibroblasts, and ultimately bone tissue necrosis.[7]

Currently, the pathogenesis of ORNJ remains incompletely elucidated, which impedes the further refinement of treatment approaches. From the perspective of basic research, the progress of disease research is to a significant extent dependent on the establishment of appropriate animal models. Over the years, various experimental animals and multiple radiotherapy protocols have been employed in ORNJ studies, each offering unique characteristics suitable for different research objectives. Firstly, regarding the selection of experimental species, small animals such as rats are widely used due to their low cost and readily available reagents.[8] In contrast, large animals like dogs and miniature pigs offer advantages in terms of better tolerance and larger body size, making them valuable for specific research needs.[9-11] However, the small mandibular volume in rat limits their applicability for surgical studies related to ORNJ, while large animals such as dogs are constrained by high costs and the lack of standardized experimental reagents. Therefore, New Zealand white rabbits have emerged as an attractive alternative due to their appropriate mandibular size, lower experimental costs, and readily available reagents. These rabbits offer advantages including controllable quality, docile temperament, good tolerance, low cost, and moderate tissue size. The anatomical structure and physiological characteristics of New Zealand white rabbits closely resemble those of humans,[12] with a bone tissue metabolic rate approximately three times that of humans, significantly reducing experimental duration. Consequently, they have been widely utilized in medical research.[13] In particular, rabbit mandible models are extensively used to simulate human jawbone lesions in maxillofacial disease studies.[14] Therefore, we propose to use New Zealand white rabbits to establish an ORNJ model and investigate its modelling methods and reliability.

Secondly, the selection of radiation doses and frequencies is a critical factor in establishing an effective model. It is essential not only to accurately simulate the clinical manifestations of radiation-induced osteonecrosis but also to ensure a high success rate of the model. Several radiation protocols have been developed for New Zealand white rabbits. However, many of these protocols involve fractionated radiation,[15,16] which our preliminary studies and literature reviews indicate significantly increase the risk of early mortality, adversely affect the overall health of the animals, reduce the success rate of the model, and compromise reproducibility.[17] Therefore, after comprehensive consideration, we conclude that single-dose radiation is more appropriate for New Zealand white rabbits. Regarding the selection of radiation dose, the conventional radiotherapy regimen for human head and neck tumours typically involves a total dose of 66-74 Gy, administered in fractions of 2 Gy each.[18] According to the formula for calculating equivalent biological dose (BED = nd / (1 + d / (α/β))), assuming an α/β value of 3 for bone tissue(11), the calculated single-fraction dose falls within the range of 16.7-17.7 Gy. To investigate the most appropriate dose, this study will examine dose gradients of 16 Gy, 18 Gy, and 20 Gy.

Based on the above, this study is aimed at establishing a radiation-induced osteonecrosis model of the mandible in New Zealand white rabbits through a single high-dose ionizing radiation, systematically exploring the effects of different radiation doses on mandibular tissues, and evaluating the inducing role of tooth extraction on this basis. This model can not only simulate the process of mandibular bone lesion in humans after radiotherapy, but also provide a reliable experimental platform for researchers to deeply understand the pathogenesis of ORNJ, explore effective prevention strategies, and optimize clinical treatment approaches. Through this study, we expect to offer new perspectives and ideas for ORNJ research, promote the development of this field, and ultimately benefit a large number of patients.

Materials and methods

Animals

Sixteen healthy female New Zealand white rabbits, aged between 3 and 4 months, were procured from the Experimental Animal Center of Guangxi Medical University, each with an average weight of approximately 2 kilograms. All the New Zealand white rabbits utilized in this study were reared at a temperature ranging from 22 to 24 °C under a 12/12-hour light/dark cycle and had unrestricted access to food and water. After a one-week acclimatization period, the 12 New Zealand white rabbits were randomly allocated to a control group (not subjected to radiation, n = 4) and three experimental groups (exposed to 16Gy, 18Gy, and 20Gy of radiation, respectively, with n=4 in each group). Throughout the entire experiment, all operations were stringently conducted in accordance with ethical principles. No rabbits were euthanized prior to the conclusion of the experiment, and no surviving individuals were detected at the end of the experiment. Additionally, this experimental protocol has been formally sanctioned by the Ethics Committee of Guangxi Medical University (No 202310008), and strictly adhered to the ARRIVE guidelines to ensure the scientificity, ethicality, and reproducibility of the study.

Radiotherapy and tooth extraction

The dose gradients were set as described above, specifically 0 Gy, 16 Gy, 18 Gy, and 20 Gy, in ascending order. Prior to

irradiating the experimental rabbits, general anaesthesia was initially induced by intravenously injecting 25% urethane (4mg/kg) through the earlobe vein, and they were subsequently appropriately immobilized. A 6MV electron linear accelerator was employed for radiation, with a radiation field size of 6cm × 6cm and a source-skin distance of 100cm. The dose rate was set at 400cGy/min. A total radiation dose of 16Gy, 18Gy, and 20Gy was respectively administered to the right mandible, while other areas were shielded using lead shielding. It is notable that the rabbits in the control group were not subjected to any radiation. In the second week following irradiation, both the experimental group and the control group rabbits were operated on under sterile conditions, and 1-2 teeth from the lower right molars were extracted. Suturing of the gums was not necessary, and the vital signs of the rabbits were closely monitored for 24 hours after the operation. Immediately after the operation, the rabbits were given a subcutaneous injection of meloxicam injection (0.3mg/kg) (Jizhongshouyao Co. Ltd, Baoding, China) to alleviate pain, and they were returned to their cages to recover naturally in the absence of active bleeding.

Micro CT

Four weeks subsequent to the extraction surgery, all the experimental rabbits were euthanized through the administration of an overdose of urethane via the auricular vein. Subsequently, the rabbits underwent a right mandibular resection and thereafter underwent Micro CT scanning (Hitachi, Japan). The region of interest (ROI) within the scanning images was delineated as the boundary of the bone tissue impacted by the extraction surgery. Once the scanning was accomplished, quantitative analyses were executed on the bone volume ratio(BV/TV), average trabecular thickness (Tb.Th), average trabecular number (Tb.N), and average trabecular spacing (Tb.Sp) of each scanning image using VGstudio MAX 2.2.2 64-bit software, and a three-dimensional reconstruction of the right mandible was carried out.

Scanning electron microscope (SEM)

Upon sampling, the specimen was promptly immersed in the fixative solution (Servicebio, Wuhan) at room temperature and fixed for 2 hours, followed by transfer to 4 °C for storage. The fixed sample was rinsed three times with 0.1M phosphate buffered saline (PB, pH7.4) at room temperature in the dark for 15 minutes each occasion. 1% osmium tetroxide in 0.1M phosphate buffered saline was fixed at room temperature in the dark for 1 - 2 hours. The sample was rinsed three times with 0.1M phosphate buffered saline at room temperature in the dark for 15 minutes each time. Subsequently, the tissue underwent dehydration, where the tissue was placed in 30% - 50% - 70% - 80% - 90% - 95% - 100% - 100% ethanol for 15 minutes each time, and euparin (Sinopharm Chemical Reagent Co., Ltd., Shanghai) for 15 minutes. Then, the sample was placed in a critical point dryer (Quorum, UK) for drying. The sample was placed on the sample stage of the Lon Sputtering Apparatus (HITACHI, Japan) with the carbon film double-sided adhesive tape adhered to it and sprayed with gold for approximately 30 seconds. The sample was observed using a scanning electron microscope (HITACHI, Japan) under a high vacuum mode (~5.10-4 Pa) at 3.0 kV accelerating voltage and at 50 μm to minimize the charge effect.

Hematoxylin and eosin (HE) staining

At room temperature, the mandible specimen was fixed in 4% paraformaldehyde (Solarbio, Beijing) for 48 hours and subsequently decalcified with 10% EDTA (Solarbio, Beijing) for 4 weeks, with the solution being replaced every other day. Subsequently, the tissue was transferred to an automatic dehydrator (Nikon, Japan) and underwent gradual dehydration in accordance with a pre-determined program, employing 70%, 80%, 90%, 95%, and 100% ethanol solutions, followed by clearing with xylene. The specimen was then embedded in a paraffin embedding machine (Hubei Kangqiang Medical Instrument Co., Ltd., Wuhan) and sliced into 4μm-thick sections using a paraffin sectioning machine (ThermoFisher, USA) for subsequent staining. Prior to staining, the sections were placed in a 60 °C incubator for 3 hours and were successively stained with hematoxylin, differentiating agent, bluing solution, and eosin dye, followed by dehydration with 70%, 85%, 95%, and 100% alcohol, and clearing with xylene before mounting. The sections were examined under a fluorescence microscope (Leica, Germany).

Masson staining

The pre-staining procedure is identical to that of HE staining. The Masson staining kit (Solarbio, Beijing) was employed for staining. In Masson staining, mature collagen fibres present as red, while immature ones exhibit a blue colour, which can facilitate our understanding of the extent of bone destruction following radiation. A 100x objective field was selected from representative sections under a brightfield microscope (Leica, Germany), and three random 200x objective fields were chosen. The area of mature collagen fibres was quantitatively analysed using ImageJ software in each group.

TRAP staining

The pre-staining process is consistent with that for HE staining. Utilize the TRAP dye solution kit (Servicebio, Wuhan) for staining. Encircle the sections with a brush and place them in a wet box. Incubate them at 37 °C with distilled water for 2 hours, discard the distilled water, and put the sections back in the wet box. Drop the filtered and freshly prepared TRAP incubation solution onto them and incubate them at 37 °C in an oven for 20 minutes. Then employ haematoxylin for counterstaining, and mount the sections in xylene and cover them with a cover slip. We randomly selected 3 fields of view at 200x magnification to count the number of TRAP-stained osteoclasts, and subsequently conducted statistical analysis on them.

TUNEL staining

TUNEL (Terminal Deoxynucleotidyl Transferase-mediated Deoxyribonucleotide Transfer Detection) was utilized for the identification of apoptosis in bone cells. All procedures were

carried out in accordance with the instructions provided in the TUNEL Assay Kit (Servicebio, Wuhan) on bone tissue sections. Subsequently, the sections were treated with proteinase K, TUNEL reaction solution, and 4′,6-diamidino-2-phenylindole (DAPI) for nuclear staining, haematoxylin for counterstaining, and ultimately, typical images were captured at 200x magnification using an inverted fluorescence microscope (Leica, Germany) for the purpose of achieving contrast.

IHC

The pre-staining procedure is identical to that of HE staining. Subsequently, the slides are baked at 60 °C for 3 to 4 hours, followed by dewaxing with xylene and rehydration with a graded alcohol sequence. The tissue is subsequently boiled in citrate buffer for antigen retrieval and cooled at room temperature. 3% hydrogen peroxide is employed as an endogenous peroxidase inhibitor and incubated at 37 °C for 30 minutes. Then, the tissue is incubated overnight with CD31 monoclonal antibody (Proteintech, China, 1:200) and TGFβ-1 monoclonal antibody (Servicebio, China, 1:200) at 4 °C. The tissue is then warmed at 37 °C for 15 minutes and incubated with the universal secondary antibody (Beijing Zhongshan Jinqiao Biotechnology Co., Ltd., Beijing) for 15 minutes. Next, DAB staining is carried out, followed by haematoxylin counterstaining, dehydration with saline alcohol, bluing with acetic acid, mounting, and observation under brightfield illumination using an inverted fluorescence microscope. For CD31 staining, we initially select typical fields of view at 100x magnification and randomly select 3 fields of view at 200x magnification to analyse the positive cell area using ImageJ software. For TGF-β1, we select typical fields of view at 200x magnification and randomly select 3 fields of view at 400x magnification to quantitatively analyse the average value for statistical analysis.

Statistical analysis

The experimental data were presented in the form of mean ± standard deviation. The data were analysed using one-way ANOVA with SPSS 25.0, and the homogeneity of variance was examined. Firstly, the overall differences were ascertained. For those with overall differences and homogeneous variance, the LSD post-hoc test was employed to calculate the differences among each group. For those with overall differences and non-homogeneous variance, the Tamhane post-hoc test was utilized to calculate the differences between groups. Quantitative analysis encompassed comparing BV/TV, Tb.Th, Tb.N, and Tb.Sp measured by micro CT between the two groups. The area of mature bone stained with Masson trichrome was quantitatively analysed using ImageJ software, and the area of positive cells stained by immunohistochemistry was evaluated. A significance level of $P \leqq .05$ was regarded as statistically significant. Subsequently, GraphPad Prism v8.0 software (Graph Pad Inc., San Diego, CA, United States) was used to generate statistical graphs.

Results

Gross anatomical inspection

Throughout the experiment, the experimental rabbits demonstrated excellent tolerance to the radiation dose, and no premature and unexpected deaths occurred. Nevertheless, one rabbit in the 20Gy group manifested right lower jaw swelling for an unclear reason. The condition improved following antibiotic treatment, and the rabbit survived normally until the conclusion of the experiment. Four weeks after tooth extraction, no hair loss was observed on the right lower jaw of the rabbits in the control group, and the right extraction site had healed completely (Figure 1A). In contrast to the control group, the rabbits in the 16Gy group exhibited mild

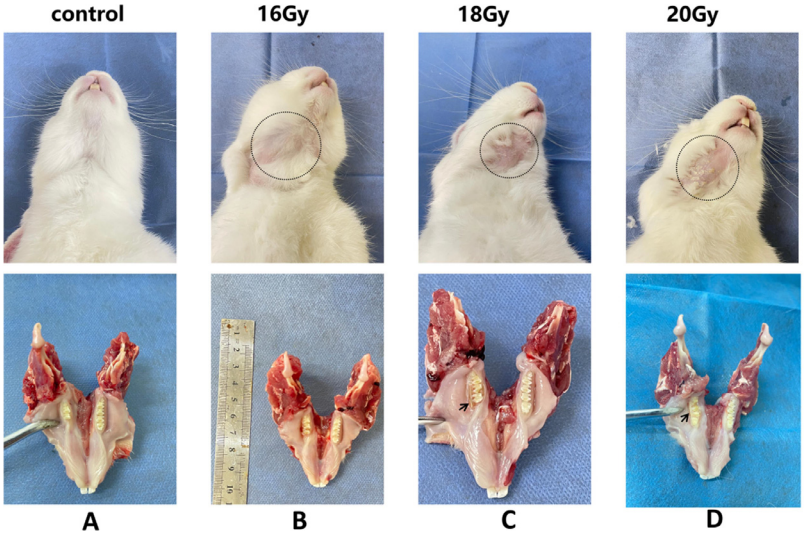

Fig. 1 – Post-extraction appearance of the rabbit right mandible 4 weeks after tooth extraction. Control group: no hair loss, good healing of extraction socket (A); 16Gy group: mild hair loss, redness and swelling of extraction socket (B); 18Gy group: obvious hair loss, non-healing of extraction socket, visible bone exposure (black arrow) (C); 20Gy group: obvious hair loss, severe and obvious bone exposure (D).

hair loss on the right lower jaw, along with redness and suboptimal healing of the extraction site (Figure 1B). The rabbits in the 18Gy and 20Gy groups presented obvious hair loss on the right lower jaw and non-healing of the extraction site, with severe exposure of the alveolar bone being grossly visible (Figure 1 C, 1D).

Micro CT analysis

We utilized Micro-CT imaging to evaluate and analyze the changes in mandibular bone quality as radiation dose increased. Regarding the bone analysis among the groups, we performed three-dimensional reconstruction of the right mandible of rabbits after Micro CT scanning and conducted quantitative analysis of the ROI regions as defined above. The three-dimensional reconstruction indicated that the mandible of each irradiated group exhibited obvious bone destruction, and no mature bone tissue was identified filling the socket resulting from tooth extraction (Figure 2A, B, C, D). The cross-sectional images of the Micro CT scans reveal that the control group exhibited better bone healing (Figure 2E). However, the bone destruction intensified with the increase in dose. At 16Gy, poor bone healing was noted in the socket bone cortex (Figure 2F). High-density and irregular dead bone was witnessed in the trabecular bone of the 16Gy, 18Gy, and 20Gy groups (Figure 2G), and the 20Gy group displayed the destruction of the buccal and lingual sides of the cortical bone (Figure 2H). The analysis results of the microstructural parameters of bone tissue demonstrate that, in terms of the overall trend, BV/TV and Tb.N increase along with the rising of the radiation dose, while the Tb.Sp value decreases. Regarding the intergroup differences, BV/TV, Tb.N, and Tb.Sp are generally distinct, as follows:[1] The BV/TV values of all radiation groups are statistically distinct from the control group ($P < .05$), and there is no disparity between the 16Gy and 18Gy groups, while significant differences exist between the other radiation groups (Figure 2I);[2] The Tb.N value of the 16Gy group is not statistically dissimilar from the control group ($P > .05$), while the 18Gy group ($P < .01$) and the 20Gy group ($P < .001$) are statistically different from the control group (Figure 2J);[3] Concerning the Tb.Sp value, there is no statistical variance between the 16Gy group, the 18Gy group and the control group ($P > .05$), while a statistically significant difference exists between the 20Gy group and the control group ($P < .001$) (Figure 2K).

SEM results

Furthermore, SEM offers a highly detailed microscopic imaging perspective to elucidate the extent of changes in

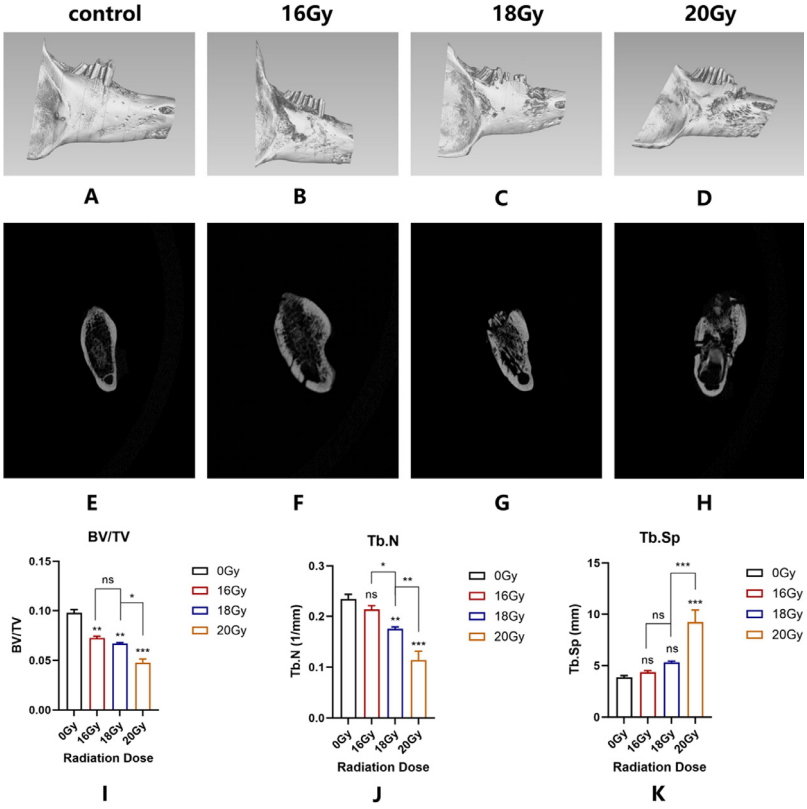

Fig. 2 – The three-dimensional reconstruction and data analysis outcomes of Micro CT. In the control group, the cortical bone was continuous and smooth, and the bone healing after tooth extraction was favorable (A); in the 16Gy group, the cortical bone was discontinuous and impaired, and the periodontal ligament was wounded (B); in the 18Gy group, the cortical bone at the tooth extraction site was significantly damaged, and the bone healing was conspicuously poor (C); in the 20Gy group, the periodontal ligament was notably damaged, the height was reduced, and the bone healing was inferior (D); the cross-sectional view of the control group on Micro CT (E); the cross-sectional view of the 16Gy group on Micro CT (F); the cross-sectional view of the 18Gy group on Micro CT (G); the cross-sectional view of the 20Gy group on Micro CT (H); the BV/TV statistical chart (I); the Tb.N statistical chart (J); the Tb.Sp statistical chart (K).

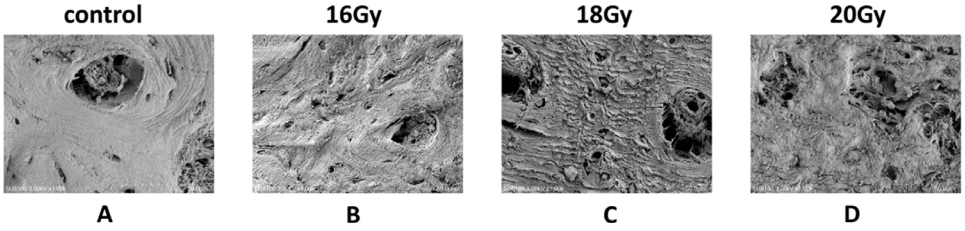

Fig. 3 – Scanning electron microscopy (SEM) observation of the surface and trabecular structure of the mandible. Control Group: Smooth surface and normal trabecular and plate-like structure (A); 16Gy Group: Rough surface and disordered trabecular arrangement (B); 18Gy Group: Even rougher surface, trabecular fracture and the formation of microcracks (C); 20Gy Group: Trabecular atrophy and fracture, severe destruction of the plate-like structure (D).

mandibular bone surface quality and trabecular arrangement. The surface of the right mandible in the control group was smooth, and the trabecular and lamellar structures of the bone were normal (Figure 3A). In contrast to the control group, the trabecular arrangement and lamellar structure of the mandible in the 16Gy group seemed disordered to a certain extent on the bone surface (Figure 3B). The roughness degree of the mandible surface in the 18Gy group was further augmented, and the trabecular arrangement was even more chaotic, with some fractures and the formation of microcracks (Figure 3C). In the 20Gy group, the trabecular arrangement was further disrupted, accompanied by bone atrophy, fractures, and the disappearance of the bone bridge. The lamellar structure was destroyed, and the continuity was lost, resulting in severe bone destruction (Figure 3D).

HE staining

From a histopathological perspective, HE staining allows for the preliminary observation of bone quality changes, inflammatory responses, and the presence of empty bone depressions in each group. The HE staining results indicated that in the control group, the extraction socket area was filled with newly formed bone tissue, the bone marrow presented a healthy state, and no fibrosis or inflammatory reaction was observed (Figure 4A). In the 16Gy group, an inflammatory reaction was noticed in the medullary cavity, and the number of empty bone depressions increased, but no obvious dead bone formation was detected (Figure 4C). In the 18Gy and 20Gy dose groups, a significant increase in the number of empty bone depressions was witnessed, and fibrosis was observed in the medullary cavity, along with obvious dead bone formation (Figure 4E, 4G).

Masson staining

Compared to HE staining, Masson staining offers a more detailed visualization of tissue architecture and enables more precise detection of collagen fibre changes in bone tissue. The Masson staining results revealed that following the increase of radiation dose in the rabbit mandible after radiation and tooth extraction, the degree of fibrosis within the medullary cavity significantly augmented. The control group exhibited mature anterograde red-stained collagen fibres (Figure 4B), while the 16Gy group manifested mild fibrosis alterations within the medullary cavity (Figure 4D). The 18Gy and 20Gy

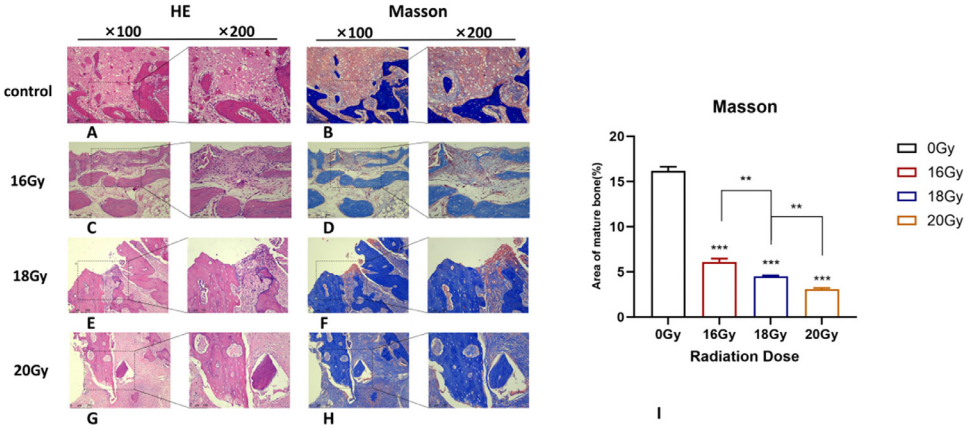

Fig. 4 – Results of HE and Masson staining. In the control group, HE staining revealed new bone formation (A) with moderate maturity (B). In the 16Gy group, HE staining indicated inflammatory reaction without obvious inflammation (C) and insufficient bone maturity (D). In the 18Gy group, the observation demonstrated a significant increase in empty lacunae and the formation of dead bone (E), and the blue immature collagen fibres were prominent (F). In the 20Gy group, obvious dead bone formation and severe bone destruction were noted (G), and the maturity of collagen fibres was decreased (H). Statistical analysis of the maturity of collagen fibres among the groups (I).

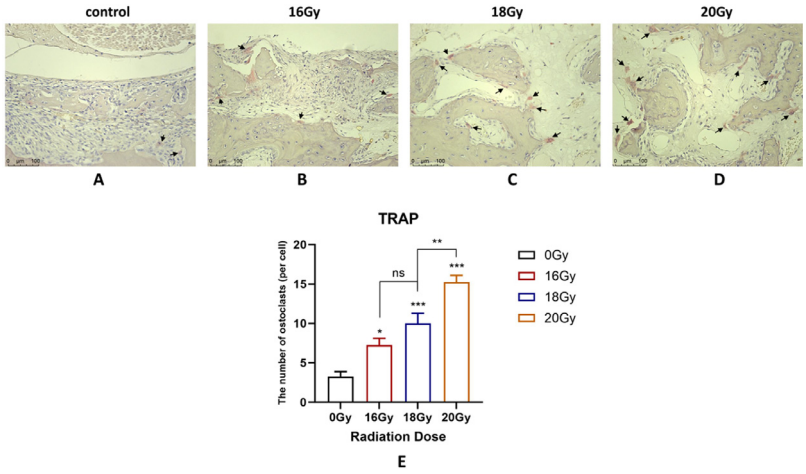

Fig. 5 – Results of TRAP staining. In the control group, merely a small quantity of osteoclasts were expressed (A); in the 16Gy group, the number of osteoclasts rose slightly (B); in the 18Gy group, the number of osteoclasts increased conspicuously (C); in the 20Gy group, the number of osteoclasts increased significantly (D). Statistical Counting of TRAP Staining (E).

groups demonstrated obvious fibrosis and notably insufficient bone maturity (Figure 4F, H). Statistically significant differences existed between the three groups and the control group ($P < .001$). Additionally, significant differences in collagen maturity were observed between the 16Gy group and the 18Gy group ($P < .01$), and between the 18Gy group and the 20Gy group ($P < .01$) (Figure 4I).

TRAP staining

The TRAP staining is capable of presenting osteoclasts as larger, multinucleated, and red-stained morphologies, facilitating the observation of osteoclast numbers across different dose levels. In the control group following tooth extraction, a small number of osteoclasts were expressed (black arrows) (Figure 5A); nonetheless, with the escalation of the radiation dose, the quantity of osteoclasts demonstrated an increasing tendency, suggesting that ionizing radiation aggravates the damage to bone tissue (Figure 5B, 5C, 5D). Counting the number of osteoclasts in the staining outcomes disclosed that a disparity was noted between the 16Gy group and the control group ($P < .05$), while statistically significant differences were witnessed between the 18Gy ($P < .001$), 20Gy ($P < .001$) groups and the control group; however, no significant difference was detected between the 16Gy group and the 18Gy group ($P > .05$), while a significant difference emerged between the 18Gy group and the 20Gy group ($P < .01$) (Figure 5E).

TUNEL staining

TUNEL staining is a molecular biology technique founded on DNA fragmentation and 3′-OH exposure during cell apoptosis. It utilizes labeled DNA ends to identify and quantify apoptotic cells, offering crucial technical support for the study of cell apoptosis. Specifically, it elucidates the damage caused by radiation to mandibular bone tissue from an apoptotic perspective. The TUNEL staining outcomes reveal that as the dose escalates, the intensity of the apoptotic signal intensifies. The 16Gy group exhibits statistically significant differences from the control group ($P < .05$), while the disparities between the 18Gy group and the 20Gy group are more pronounced ($P < .01$) (Figure 6).

IHC results

CD31

Immunohistochemical CD31 staining is localized to endothelial cells and can be employed to assess variations in the number of blood vessels and reflect the blood supply during the process of tissue repair following radiation exposure. In comparison with the control group, the mandibles of the rabbits in the experimental group demonstrated a gradual reduction in the number of blood vessels with an increasing radiation dose, accompanied by no obvious yellow staining (Figure 7A, 7C, 7E, 7G). There existed a statistically significant difference between the radiation groups and the control group ($P < .001$), and the disparity between different dose groups remained significant ($P < .001$) (Figure 7I).

TGF-β1

Immunohistochemical staining of TGFβ-1 was localized within the cytoplasm of osteoblasts in bone tissue, and a low level of expression was also observed in bone cells, which could be utilized to demonstrate the fibrotic trend of bone tissue after irradiation. It can be seen from the TGF-β1 staining images that only a small quantity of endogenous expression was present in the control group (Figure 7B). Meanwhile, the number of yellow-stained osteoblasts increased in the 16Gy group (Figure 7D), and the expression of TGF-β1 significantly augmented in the 18Gy group and 20Gy group (Figure 7F, 7H). It can be discerned from the pictures and quantitative data that only a minor amount of expression is present in the control group, while the expression levels of the other three groups increase gradually. The differences among the groups are all statistically significant ($P < .001$) (Figure 7I).

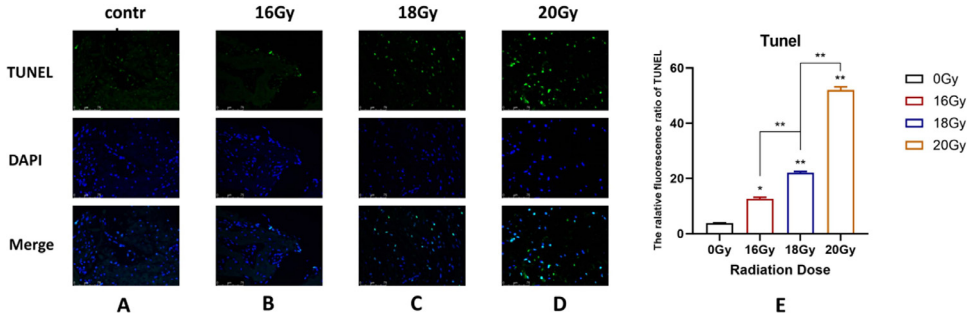

Fig. 6 – Outcomes of TUNEL staining. The control group presents less apoptotic signal fluorescence (A); the 16Gy group exhibits only a slight expression of apoptosis (B); the 18Gy group demonstrates a marked increase in apoptosis (C); the 20Gy group reveals a significant enhancement in the expression of the apoptotic signal green fluorescence (D); Statistical analysis of the relative fluorescence intensity of TUNEL staining (E).

Discussion

Radiotherapy, being one of the common therapeutic approaches for malignant diseases of the head and neck, not only eliminates tumor cells but also inflicts varying degrees of harm to normal tissue cells through mechanisms such as direct penetration or the "bystander effect".[19-21] Among the numerous acute and chronic adverse reactions elicited by ionizing radiation, the most severe is the radiation-induced osteonecrosis of the jaw (ORNJ), which constitutes a clinical conundrum that demands urgent resolution.[22,23] Current research indicates that although the incidence of ORNJ has declined with the establishment of individualized radiotherapy, it still maintains a certain level, approximately 8%, due to chronic infection, pain, dysphagia, and facial deformity, thereby significantly impacting the quality of life of patients.[24] It is notable that there exist numerous urgent issues that require resolution in the current studies on ORNJ. Hence, for the purposes of exploring the etiology and preventing the disease, establishing a simple and reliable animal model for symptomatic research represents the initial and most crucial step.

This study selected New Zealand white rabbits as the experimental model for single high-dose irradiation followed by tooth extraction to simulate ORNJ. Firstly, compared to smaller animals such as rats, New Zealand white rabbits possess larger mandibles, which provide advantages in micro-CT imaging and other analyses.[25] Additionally, the larger mandibular tissue in rabbits is more suitable for surgical treatment studies of ORNJ,[26,27] better accommodating subsequent in situ tissue requirements. This choice also considers factors such as animal tolerance, quality control, and experimental cost.[12] However, while dogs and miniature pigs possess sufficiently large mandibular bone tissues, they are associated with high costs and pose challenges in control. Additionally, adhering to the principles of experimental animal protection and aiming to minimize confounding factors such as pre-radiotherapy general anaesthesia and animal transportation, a single radiotherapy session could potentially achieve the objective of simulating radiation-induced osteonecrosis of the jawbone. Compared to fractionated radiotherapy, this approach may reduce time costs and lower the risk of adverse outcomes due to general

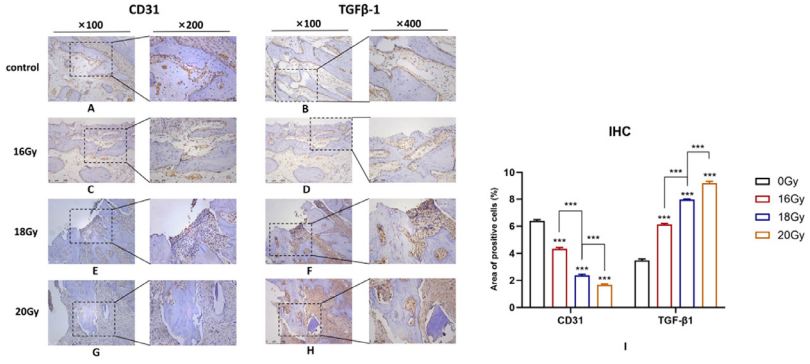

Fig. 7 – Outcomes of IHC staining. In the control group, there was abundant angiogenesis and CD31 was conspicuously yellow-stained (A), while TGF-β1 had merely some endogenous expression (B); in the 16Gy group, there was a certain amount of neovascularization (C), and fibrosis was evident (D); in the 18Gy group, neovascularization was markedly decreased (E), and fibrosis was obvious (F); in the 20Gy group, the vessels were severely damaged (G), and the fibrosis phenomenon was significant (H); The quantitative analysis results of IHC images (I).

anaesthesia or external environmental stressors for the animals, thereby facilitating the establishment of a more reliable animal model. Finally, multiple studies have demonstrated that tooth extraction after irradiation is one of the most common causes of ORNJ,[28-30] and thus we employed the removal of the right lower molar teeth two weeks after irradiation as the trigger factor for ORNJ.

To more comprehensively evaluate the model construction and gain a deeper understanding of the transformation states of ORNJ disease, we conducted a multi-faceted analysis involving gross observation, imaging studies, and pathological examinations. These methods were used in concert to cross-validate findings and facilitate detailed discussions. The experimental results indicate that single-dose radiation of 18Gy and 20Gy can induce the occurrence of ORNJ, which can be affirmed by gross observation, imaging, and pathological examination. Firstly, gross observation reveals hair loss, obvious bone exposure, and poor healing of extraction sockets. In contrast, the control group shows good healing. Although there is slight hair loss in the 16Gy group, the degree of bone exposure is not prominent, and overall healing is superior to the two higher-dose groups. For imaging data, we employed Micro CT and scanning electron microscopy methods, which jointly demonstrate that as the dose increases, the degree of poor bone healing deteriorates, the trabecular bone becomes disordered, the cortical bone surface becomes rougher, the periodontal interval is disrupted, and scattered high-density images appear in the socket. All these indicate a positive correlation between the increase in dose and the severity or stage of ORNJ.

It is noteworthy that for numerous years, researchers have been focusing on the alterations in the histopathology of ORNJ during its progression. From Marx's three-low theory to Delainan's widely accepted "fibrosis theory," the key points have mainly concentrated on "increased inflammation," "vascular injury," "fibrosis," and "bone loss." Among these, vascular injury may play a pivotal role in the pathogenesis of ORNJ, and vascular atrophy has a profound influence on bone remodelling and fibrosis processes.[31] Furthermore, local microvascular changes and injuries may be more prominent than those of large vessels,[32] and microvascular damage has been observed in the histopathology even prior to bone destruction.[10] Studies have demonstrated that endothelial cell loss persists for several months following radiation therapy,[33] and this loss and dysfunction can severely impact vascular remodelling in the irradiated area, resulting in oxygen deprivation in bone tissue and influencing the quantity and activity of osteoblasts, thereby destroying the quality and blood supply of the mandibular bone and contributing to the further occurrence and progression of ORNJ. In our experiments, we employed CD31 immunohistochemical staining to reveal that radiation affects the formation of new microvessels, and the phenomenon becomes more pronounced with an increasing dose, accompanied by a significant reduction in the number of new vessels; while HE staining indicated that inflammation and fibrosis varied with the dose, with an increase in dead bone formation and empty bone lacunae. Specific staining methods such as Masson staining, TRAP staining, and TUNEL staining manifested that the radiation dose affects the immaturity of new collagen fibres, enhanced the activity of osteoclasts, and increased cell apoptosis, which is consistent with the finding that ionizing radiation can induce osteoclast differentiation and bone resorption by Jian Zhang et al.[34]

Meanwhile, transforming growth factor beta 1 (TGF-β1) primarily undertakes the role of regulating the proliferation and differentiation of fibroblasts, and fibrosis exerts a widespread influence on bone and surrounding soft tissues following radiation exposure, which constitutes a concomitant cause of ORNJ.[35] We discovered that the expression of TGF-β1 in the cytoplasm of osteoblasts rose with the increase of the dose, further affirming the positive correlation between ionizing radiation and fibrosis.

In conclusion, this study initially employed single-dose irradiations of 16Gy, 18Gy, and 20Gy and extracted teeth two weeks after irradiation to induce ORNJ. To verify the established simulation model, we utilized multiple detection approaches, including Micro CT imaging and scanning electron microscopy, which mainly verified from the perspective of bone destruction. In terms of histopathology, HE staining, Masson staining, TUNEL staining, TRAP staining, and immunohistochemistry with CD31 and TGF-β1 staining were employed to explore the severity and pathogenesis of ORNJ from various aspects such as cell apoptosis, osteoclast metabolism, vascular injury, and fibrosis formation. The results of each method were mutually confirmatory, avoiding the randomness and unreliability of a single detection outcome and highlighting the advantages and characteristics of each method. Based on this, we contend that irradiating the mandible of New Zealand white rabbits with a single dose of 18Gy and extracting teeth two weeks after irradiation is adequate for constructing a model of radiation-induced osteonecrosis of the jaw.

However, our study still possesses certain limitations. Firstly, due to diverse factors, our study employed 16 New Zealand white rabbits, and the quantity might still be inadequate. Secondly, although a single radiation dose is sufficient to induce ORNJ, whether it can effectively simulate the pathophysiological process of ORNJ in clinical patients remains to be explored, which is also one of the issues that animal models commonly need to confront. Furthermore, the observation time point in our experiment was one month after tooth extraction, and the long-term change level still requires further investigation. Future experiments can be designed more comprehensively, and the observation period can be determined based on different research requirements. Meanwhile, incorporating additional osteoclast-related biomarkers such as RANKL and OPG can provide a more comprehensive and accurate characterization of the disease process, thereby facilitating the validation of hypotheses related to etiology or treatment efficacy.

In conclusion, this study suggests the application of a single total dose of 18Gy radiation for the establishment of a radiation-induced osteonecrosis model in New Zealand white rabbits, with the hope of laying a beneficial experimental basis for the exploration of the etiology of ORNJ and disease prevention and control.

Availability of data and materials

The datasets generated during and analysed during the current study are available from the corresponding author on reasonable request.

Funding

This work was supported by the "Innovation Project of Guangxi Graduate Education" (YCSW2024263).

Authors' contributions

D.Y.W. is responsible for conceptualization and funding acquisition. Y.T.W. is responsible for methodology, formal analysis and writing original draft. X.W. is responsible for methodology, supervision and formal analysis. Z.Q.L. is responsible for validation and writing review and editing. H.Y.L. and D.Q.M. are responsible for investigation and resources.

Conflicts of interest

None disclosed.

Acknowledgements

We would like to express our gratitude for the invaluable support provided by the Experimental Animal Center of Guangxi Medical University.

REFERENCES

1. Siegel RL, Giaquinto AN, Jemal A. Cancer statistics, 2024. CA: Cancer J Clin 2024;74(1):12–49.
2. Jham BC, da Silva, Freire AR. Oral complications of radiotherapy in the head and neck. Braz J Otorhinolaryngol 2006;72 (5):704–8.
3. Li Y, Wang X, Pang Y, Wang S, Luo M, Huang B. The potential therapeutic role of mesenchymal stem cells-derived exosomes in osteoradionecrosis. J Oncol 2021;2021:4758364.
4. Jacobson AS, Buchbinder D, Hu K, Urken ML. Paradigm shifts in the management of osteoradionecrosis of the mandible. Oral Oncol 2010;46(11):795–801.
5. Støre G, Eribe ER, Olsen I. DNA-DNA hybridization demonstrates multiple bacteria in osteoradionecrosis. Int J Oral Maxillofac Surg 2005;34(2):193–6.
6. Marx RE. Osteoradionecrosis: a new concept of its pathophysiology. J Oral Maxillofac Surg 1983;41(5):283–8.
7. Delanian S, Lefaix JL. The radiation-induced fibroatrophic process: therapeutic perspective via the antioxidant pathway. Radiother Oncol 2004;73(2):119–31.
8. Liu S, Zhang B, Ma S, Wu F, Shi X, Wu J, et al. The mechanism of bone metabolism in a Sprague Dawley rat model of mandibular osteoradionecrosis. Quant Imaging Med Surg 2024;14 (7):4403–16.
9. Poort LJ, Ludlage JHB, Lie N, Böckmann RA, Odekerken JCE, Hoebers FJ, et al. The histological and histomorphometric changes in the mandible after radiotherapy: an animal model. J Craniomaxillofac Surg 2017;45(5):716–21.
10. Xu J, Zheng Z, Fang D, Gao R, Liu Y, Fan ZP, et al. Early-stage pathogenic sequence of jaw osteoradionecrosis in vivo. J Dent Res 2012;91(7):702–8.
11. Zhou Z, Lang M, Fan W, Dong X, Zhu L, Xiao J, et al. Prevention of osteoradionecrosis of the jaws by low-intensity ultrasound in the dog model. Int J Oral Maxillofac Surg 2016;45(9):1170–6.
12. Zong C, Cai B, Wen X, Alam S, Chen Y, Guo Y, et al. The role of myofibroblasts in the development of osteoradionecrosis in a newly established rabbit model. J Craniomaxillofac Surg 2016;44(6):725–33.
13. Abu-Serriah MM, McGowan DA, Moos KF, Bagg J. Extra-oral craniofacial endosseous implants and radiotherapy. Int J Oral Maxillofac Surg 2003;32(6):585–92.
14. Shah SR, Young S, Goldman JL, Jansen JA, Wong ME, Mikos AG. A composite critical-size rabbit mandibular defect for evaluation of craniofacial tissue regeneration. Nat Protoc 2016;11(10):1989–2009.
15. Ruaro A, Taboni S, Chan HHL, Mondello T, Lindsay P, Komal T, et al. Development of a preclinical double model of mandibular irradiated bone and osteoradionecrosis in New Zealand rabbits. Head Neck 2025;47(2):625–34.
16. Zhang WB, Zheng LW, Chua D, Cheung LK. Bone regeneration after radiotherapy in an animal model. J Oral Maxillofac Surg 2010;68(11):2802–9.
17. Yamasaki MC, Roque-Torres GD, Peroni LV, Nascimento EHL, Salmon B, Oliveira ML, et al. A modified protocol of mandibular osteoradionecrosis induction in rats with external beam radiation therapy. Clin Oral Investig 2020;24(4):1561–7.
18. Alfouzan AF. Radiation therapy in head and neck cancer. Saudi Med J 2021;42(3):247–54.
19. Barazzuol L, Coppes RP, van Luijk P. Prevention and treatment of radiotherapy-induced side effects. Mol Oncol 2020;14 (7):1538–54.
20. Parisi S, Napoli I, Lillo S, Cacciola A, Ferini G, Iatì G, et al. Spine eburnation in a metastatic lung cancer patient treated with immunotherapy and radiotherapy. The first case report of bystander effect on bone. J Oncol Pharm Pract 2022;28(1):237–41.
21. Daguenet E, Louati S, Wozny AS, Vial N, Gras M, Guy JB, et al. Radiation-induced bystander and abscopal effects: important lessons from preclinical models. Br J Cancer 2020;123(3):339–48.
22. Watson EE, Hueniken K, Lee J, Huang SH, El Maghrabi A, Xu W, et al. Development and standardization of an osteoradionecrosis classification system in head and neck cancer: implementation of a risk-based model. J Clin Oncol 2024;42 (16):1922–33.
23. Naseer A, Goode F, Doyle T. Osteoradionecrosis - an old problem with new consequences. Curr Opin Support Palliat Care 2024;18(1):39–46.
24. Fitzgerald KT, Lyons C, England A, McEntee MF, Devine A, O'Donovan T, et al. Risk factors associated with the development of osteoradionecrosis (ORN) in head and neck cancer patients in Ireland: a 10-year retrospective review. Radiother Oncol 2024;196:110286.
25. Dos Santos M, Demarquay C, Ermeneux L, Aberkane F, Bléry P, Weiss P, et al. Refining the mandibular osteoradionecrosis rat model by in vivo longitudinal μCT analysis. Sci Rep 2021;11 (1):22241.
26. Wang X, Wang Y, Li Y, Lu H, Mo D, Liu Z, et al. The initial implementation of the transverse bone transport technique in the post-radiation region of the mandible. A pre-clinical in vivo study. BMC Oral Health 2024;24(1):1434.
27. Singh A, Kitpanit S, Neal B, Yorke E, White C, Yom SK, et al. Osteoradionecrosis of the jaw following proton radiation therapy for patients with head and neck cancer. JAMA Otolaryngol Head Neck Surg. 2023;149(2):151–9.
28. Vahidi N, Lee TS, Daggumati S, Shokri T, Wang W, Ducic Y. Osteoradionecrosis of the midface and mandible:

pathogenesis and management. Semin Plast Surg 2020;34 (4):232–44.
29. Balermpas P, van Timmeren JE, Knierim DJ, Guckenberger M, Ciernik IF. Dental extraction, intensity-modulated radiotherapy of head and neck cancer, and osteoradionecrosis: a systematic review and meta-analysis. Strahlentherapie und Onkologie: Organ der Deutschen Rontgengesellschaft [et al] 2022;198(3):219–28.
30. Pereira IF, Firmino RT, Meira HC, Vasconcelos BC, Noronha VR, Santos VR. Osteoradionecrosis prevalence and associated factors: a ten years retrospective study. Medicina oral, patologia oral y cirugia bucal 2018;23(6): e633–e8.
31. Peterson DE, Koyfman SA, Yarom N, Lynggaard CD, Ismaila N, Forner LE, et al. Prevention and management of osteoradionecrosis in patients with head and neck cancer treated with radiation therapy: ISOO-MASCC-ASCO guideline. J Clin Oncol 2024;42(16):1975–96.
32. Dekker H, Bravenboer N, van Dijk D, Bloemena E, Rietveld DHF, Ten Bruggenkate CM, et al. The irradiated human mandible: a quantitative study on bone vascularity. Oral Oncol 2018;87:126–30.
33. Li Y, Zhou Z, Xu S, Jiang J, Xiao J. Review of the pathogenesis, diagnosis, and management of osteoradionecrosis of the femoral head. Med Sci Monit 2023;29:e940264.
34. Zhang J, Zheng L, Wang Z, Pei H, Hu W, Nie J, et al. Lowering iron level protects against bone loss in focally irradiated and contralateral femurs through distinct mechanisms. Bone 2019;120:50–60.
35. Lyons AJ, West CM, Risk JM, Slevin NJ, Chan C, Crichton S, et al. Osteoradionecrosis in head-and-neck cancer has a distinct genotype-dependent cause. Int J Radiat Oncol Biol Phys 2012;82(4):1479–84.